PERGAMON

International Journal of Heat and Mass Transfer 44 (2001) 721–732

International Journal of HEAT and MASS TRANSFER

www.elsevier.com/locate/ijhmt

Finite-wall effect on buoyant convection in an enclosure with pulsating exterior surface temperature

Kwang Hyo Chung[a], Ho Sang Kwak[b], Jae Min Hyun[a,*]

[a]*Department of Mechanical Engineering, Korea Advanced Institute of Science and Technology, 373-1 Kusong-dong, Yusong-gu, Taejon 305-701, South Korea*

[b]*School of Mechanical Engineering, Kumoh National University of Technology, 188 Shinpyeong-dong, Kumi-shi, Kyungsangbuk-do 730-701, South Korea*

Received 3 September 1999; received in revised form 7 April 2000

Abstract

A numerical study is made of the finite-wall effect in the benchmark-configuration buoyant convection in a square cavity at large Rayleigh number. A general formulation, with one vertical sidewall of finite thickness and thermal conductivity, is presented. Firstly, the finite-wall effect for the case of non-pulsating boundary temperature condition is delineated. The energy balance consideration, together with the preceding empirical correlations, leads to a simple formula to predict the temperature at the interior surface of the finite-thickness wall. The analytical predictions are shown to be consistent with the results of full-dress Navier–Stokes numerical solutions. Secondly, the finite-wall effect for the case of pulsating boundary temperature condition is explored. The numerical results illustrate that the amplitude of oscillating Nusselt number, $A(Nu)$, at the central plane peaks at a particular pulsation frequency. This has been interpreted to be a manifestation of resonance. The finite-wall effect on the shift of resonance frequency is discussed. The temperature oscillation at the interior surface of the solid wall is examined, and the convection-modified model is introduced to describe the alteration in the temperature contrast across the fluid portion. The estimation of the resonance frequency, based on the internal gravity oscillations, is shown to be in accord with the Navier–Stokes numerical solutions. © 2001 Published by Elsevier Science Ltd.

1. Introduction

Buoyancy-driven convection in an enclosure constitutes a classical problem. In particular, convection in a square cavity, with its two vertical sidewalls maintained at different but constant temperatures, poses a benchmark configuration ([1]). Steady flow and heat transfer characteristics have been thoroughly documented for large system Rayleigh numbers $Ra \gg 1$, which are relevant to technological applications.

Recent studies have dealt with the buoyant convection when the imposed thermal boundary conditions are periodic in time [2–9]. Specifically, the responses of the confined fluid, when the heat flux or the temperature specified at one vertical wall varies periodically, are of concern. Numerical simulations and experiments have established that the buoyancy-driven convective activity in the cavity is intensified at certain discrete frequencies of the oscillation of the boundary condition. This has been termed resonance, which is characterized by attain-

* Corresponding author. Tel.: +82-42-8693012; fax: +82-42-8693210.

E-mail address: jmhyun@cais.kaist.ac.kr (J.M. Hyun).

0017-9310/01/$ - see front matter © 2001 Published by Elsevier Science Ltd.
PII: S0017-9310(00)00143-5

Nomenclature

A_r	cavity aspect ratio ($\equiv H/L$)
A_W	non-dimensional wall thickness ($\equiv D/L$)
C	specific heat at constant pressure
C_i	strength of stratification
D	thickness of the solid wall
f	dimensional frequency of the exterior-wall temperature oscillation
f_m	modifying factor
g	acceleration due to gravity
H	height of the cavity
k, k_r	thermal conductivity, thermal conductivity ratio ($\equiv k_s/k_f$)
L	length of the fluid region
N	Brunt–Väisälä frequency
Nu	average Nusselt number
p, P	dimensional, dimensionless pressure ($\equiv (p+\rho_o g y)H^2/\rho_o \kappa^2 Ra\,Pr$)
Pr	Prandtl number (ν/κ)
Ra	external Rayleigh number ($\equiv \alpha g(T_e - T_C)H^3/\nu\kappa$)
Ra_i	internal Rayleigh number ($\equiv \alpha g(T_i - T_C)H^3/\nu\kappa$)
S_C	non-dimensional thermal conductance ($\equiv k_r/A_W$)
t	dimensional time
T	dimensional temperature
T_C	temperature at the cold wall
ΔT	temperature difference ($\equiv (T_e - T_C)$)
ΔT_e	amplitude of the wall temperature oscillation at the exterior surface
ΔT_i	amplitude of the wall temperature oscillation at the interior surface
u, v	velocity components
U, V	dimensionless velocity components ($\equiv (u, v)(Ra\,Pr)^{-1/2}H/\kappa$)
x, y	coordinates
X, Y	dimensionless coordinates ($\equiv x/H, y/H$)

Greek symbols

α	volumetric expansion coefficient
β	temperature transfer ratio ($\equiv (T_i - T_C)/(T_e - T_C)$)
ε	dimensionless amplitude of the wall temperature oscillation ($\equiv \Delta T_e/\Delta T$)
ε_d	dimensionless amplitude of temperature oscillation in the solid wall
γ	phase shift of wall temperature oscillation
κ	thermal diffusivity
ν	kinematic viscosity
ρ	density
$(\rho C)_r$	heat capacity ratio ($\equiv (\rho C)_s/(\rho C)_f$)
θ	dimensionless temperature ($\equiv (T - T_C)/T_e - T_C)$)
τ	dimensionless time ($\equiv t(Ra\,Pr)^{1/2}\kappa/H^2$)
τ_d	conductive time scale of the solid wall
τ_p	dimensionless period of the wall temperature oscillation
ω	dimensionless frequency of the wall temperature oscillation ($\equiv f/N$)
ω_r	resonance frequency

Subscripts

f	fluid
e, ext	exterior surface of the solid wall
i, int	interior surface of the solid wall
r	ratio of solid property to fluid property
s	solid
o	reference

ing the maximum amplitude of heat transfer rate through the vertical midplane of the cavity [3]. For the cavity configuration in which a periodic heat flux was imposed on one vertical wall, while the other wall was at constant temperature, Lage and Bejan [3] demonstrated the existence of resonance. Also, the resonance frequency was estimated by matching the period of the oscillation of the boundary condition to the circulation time of a fluid wheel within the enclosure. The resonance frequency thus obtained was shown to be in order-of-magnitude agreement with the numerical results. In a similar development, Kwak and Hyun [7] made an in-depth re-examination of the cavity model originally proposed by Kazmierczak and Chinoda [2]. The temperature at the cold vertical wall was constant, and the temperature at the hot vertical wall varied periodically with frequency ω. Numerical solutions illustrated the presence of resonance, and the resonance frequency was found by searching for the basic mode of internal gravity oscillation in the interior region [8,9]. In summary, the resonance phenomenon in confined buoyant convection points to potentially innovative thermal technological devices, which could lead to significant management/enhancement techniques of heat transfer.

In an effort to move closer to realism, it is proposed here to study the effect of finite thickness and imperfect thermal conductivity of the boundary wall. The canonical model of de Vahl Davis [1], Kazmierczak and Chinoda [2] and Kwak and Hyun [7] takes the vertical wall of the cavity to be an infinitely thin and perfectly conducting plate. Therefore, in realistic engineering situations, an investigation is warranted to delineate the finite-wall effect on the fluid response to the externally applied periodic temperature condition. In particular, the above-described resonance phenomenon under practical circumstances is worthy of a systematic evaluation.

The finite-wall effect was addressed mostly in the context of steady-state buoyant convection problems, largely by relying on numerical solutions [10–13]. In the present work, numerical studies was made to depict the time-dependent buoyant convection in a square, subject to a periodically varying temperature condition imposed at the exterior surface of a vertical wall of finite thickness and thermal conductivity. Pertinent dimensionless parameters are identified, and the main characteristics of oscillating heat transfer are ascertained, in particular, in reference to the resonance phenomenon.

In the first stage, the general formulation and results for non-pulsating boundary temperature conditions are presented. Next, the results for pulsating boundary temperature conditions will be addressed.

2. The model

The flow layout is sketched in Fig. 1. A rectangular cavity of width L and height H is filled with a Boussinesq fluid, which satisfies the linear density-temperature relation, i.e. $\rho = \rho_o[1-\alpha(T-T_o)]$. The top and bottom horizontal walls are thermally insulated, and the cold left wall is maintained at temperature T_C. The hot right wall is of thickness D, and at the exterior surface of this wall, the pulsating temperature $T_{ext} = T_e + \Delta T_e \sin ft$ is imposed. The externally controllable temperature difference ΔT $(\equiv T_e - T_C) > 0$, and ΔT_e and f, respectively, denote the amplitude and frequency of the oscillating part of the exterior surface temperature. The physical properties are taken to be constant at the reference temperature T_o $[\equiv (T_e + T_C)/2]$.

For the fluid, the governing time-dependent Navier–Stokes equations, in properly non-dimensionalized form, read

$$\frac{\partial U}{\partial X} + \frac{\partial V}{\partial Y} = 0, \tag{1}$$

$$\frac{\partial U}{\partial \tau} + U\frac{\partial U}{\partial X} + V\frac{\partial U}{\partial Y} = -\frac{\partial P}{\partial X} + \left(\frac{Pr}{Ra}\right)^{1/2}\left[\frac{\partial^2 U}{\partial X^2} + \frac{\partial^2 U}{\partial Y^2}\right], \tag{2}$$

$$\frac{\partial V}{\partial \tau} + U\frac{\partial V}{\partial X} + V\frac{\partial V}{\partial Y} = -\frac{\partial P}{\partial Y} + \left(\frac{Pr}{Ra}\right)^{1/2}\left[\frac{\partial^2 V}{\partial X^2} + \frac{\partial^2 V}{\partial Y^2}\right] + \theta, \tag{3}$$

$$\frac{\partial \theta}{\partial \tau} + U\frac{\partial \theta}{\partial X} + V\frac{\partial \theta}{\partial Y} = \left(\frac{1}{Ra\,Pr}\right)^{1/2}\left[\frac{\partial^2 \theta}{\partial X^2} + \frac{\partial^2 \theta}{\partial Y^2}\right]. \tag{4}$$

For the solid wall, the temperature equation is

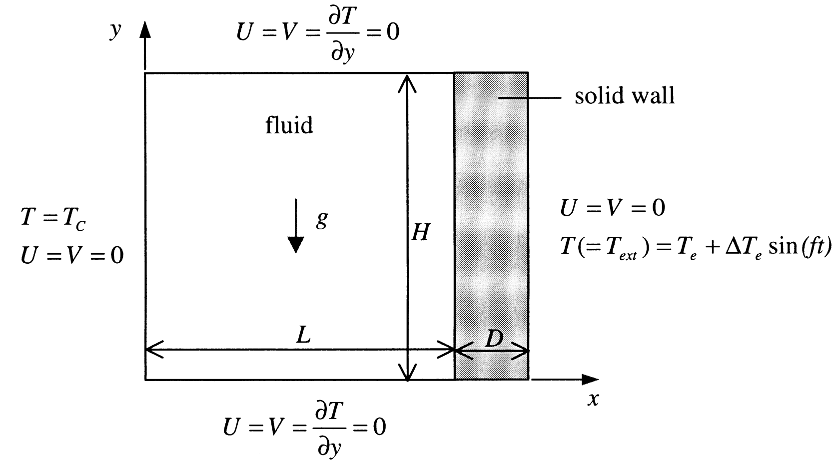

Fig. 1. Schematic of flow configuration.

$$\frac{\partial\{(\rho C)_r\theta\}}{\partial\tau} = k_r\left(\frac{1}{Ra\,Pr}\right)^{1/2}\left[\frac{\partial^2\theta}{\partial X^2} + \frac{\partial^2\theta}{\partial Y^2}\right]. \tag{5}$$

The associated boundary conditions are

$$U = V = \frac{\partial\theta}{\partial Y} = 0 \qquad \text{at } Y = 0, 1; \tag{6a}$$

$$U = V = \theta = 0 \qquad \text{at } X = 0; \tag{6b}$$

$$U = V = 0, \qquad \theta = 1 + \varepsilon\sin(\omega\tau) \qquad \text{at} \quad X = \frac{1 + A_\mathrm{W}}{A_r} \tag{6c}$$

$$\theta_\mathrm{s} = \theta_\mathrm{f},\, k_\mathrm{s}\left.\frac{\partial\theta}{\partial X}\right)_\mathrm{solid} = k_\mathrm{f}\left.\frac{\partial\theta}{\partial X}\right)_\mathrm{fluid} \qquad \text{at } X = 1/A_r. \tag{6d}$$

In the above, the non-dimensionalization schemes were the same as in Kwak and Hyun [7]; i.e.

$$\tau = t(Ra\,Pr)^{1/2}\,\frac{\kappa}{H^2}, \quad (X, Y) = \frac{(x, y)}{H}, \quad (U, V) = (u, v)(Ra\,Pr)^{-1/2}\,\frac{H}{\kappa}, \quad \theta = \frac{T - T_\mathrm{C}}{T_\mathrm{e} - T_\mathrm{C}}, \quad P = \frac{(p + \rho_\mathrm{o}gy)H^2}{\rho_\mathrm{o}\kappa^2 Ra\,Pr} \tag{7}$$

Notice that time has been made dimensionless by using the reciprocal of the representative Brunt–Väisälä frequency, N, which is defined as

$$N \equiv \left[\frac{\alpha g(T_\mathrm{e} - T_\mathrm{C})}{H}\right]^{1/2} = (Ra\,Pr)^{1/2}\,\frac{\kappa}{H^2}. \tag{8}$$

In the course of non-dimensionalization, the dimensionless parameters emerge: the Rayleigh number, $Ra = \alpha g(T_\mathrm{e} - T_\mathrm{C})H^3/\nu\kappa$; the Prandtl number, $Pr = \nu/\kappa$; the ratio of thermal conductivities, $k_\mathrm{r} \equiv k_\mathrm{s}/k_\mathrm{f}$; the ratio of thermal capacities, $(\rho C)_r \equiv (\rho C)_\mathrm{s}/(\rho C)_\mathrm{f}$; the cavity aspect ratio $A_r \equiv H/L$; the non-dimensional wall thickness $A_\mathrm{W} \equiv D/L$; the dimensionless amplitude (ε) and frequency (ω) of oscillation of the exterior surface temperature, $\varepsilon \equiv \Delta T_\mathrm{e}/(T_\mathrm{e} - T_\mathrm{C})$; $\omega \equiv f/N$.

The above equations were solved numerically by adopting the finite volume method, utilizing the well-established SIMPLER algorithm [14]. The non-linear advection terms were discretized by using the QUICK scheme [15], and the SIP solver [16] was incorporated in solving the discretized equations. Typically, a staggered grid network of (82 × 62) was deployed in the x–y plane for the fluid; for the solid wall, the grid points were (20 × 62). Grid points were clustered in the vicinities of the horizontal and vertical walls as well as near the exterior and interior surfaces of the solid wall. In the present solution procedures, a conjugate-type problem was cast for the combined domain of fluid and solid. In the solid portion, the viscosity was set to have a very large value, and, therefore, the velocity practically vanishes. The computational time step was $\Delta\tau = 2\pi/(1000\omega)$, and an even smaller value of $\Delta\tau$ was employed when ω was small. At each time step, convergence was declared when the relative differences in U, V and θ between two successive iterations fell below 10^{-4}. The quasi-steady periodic flow was judged to have been attained when the average Nusselt numbers at the cold wall ($X = 0$), mid-plane ($X = 0.5/A_r$), interior surface ($X = 1/A_r$) and exterior surface ($X = (1 + A_\mathrm{W})/A_r$) of the hot wall differed less than 10^{-3} from the corresponding values at the previous cycle. As remarked, only the quasi-steady periodic flows are of concern, and the transitory approach to this quasi-periodic state is not of primary interest. In order to ascertain the accuracy and robustness of the present numerical methodology, wide-ranging grid- and time-step convergence tests were executed. Also, calculations were repeated for the problems for which published results were available for comparison [7,10,13] both for steady and time-dependent flows. The outcome of this exhaustive series of tests and cross-comparisons proved the effectiveness and reliability of the present numerical techniques.

The following parameters were fixed in order to focus on the time-dependency of the flow, i.e. $Ra = 10^7$; $Pr = 0.7$; $(\rho C)_r = 1$; $A_r = 1$; $A_\mathrm{W} = 0.1$; $\varepsilon = 1$; $0.1 \le k_r \le 100$; and $10^{-2} \le \omega \le 100$ (see, Kwak et al. [8], Chung and Hyun [13]). The values of k_r in technological applications range from 2.8×10^{-3} (silica aerogel/mercury) to 1.4×10^5 (diamond/freon-12). The value $k_r = 0.1$ may be found in wood/water combinations. In the present efforts, the purpose is to understand the fundamentals of transport phenomena as influenced by pertinent flow parameters, rather than acquiring practically useful engineering data.

It is advantageous to introduce the definitions below to describe the time-dependent process [7]:

$$\phi^* \equiv \frac{\phi - \phi_\mathrm{ss}}{\phi_\mathrm{ss}}, \quad A(\phi) \equiv \frac{\mathrm{Max}\{\phi(\tau)\} - \mathrm{Min}\{\phi(\tau)\}}{2}$$

$$\text{for} \quad \tau_0 \le \tau \le \tau_0 + \frac{2\pi}{\omega}, \quad \bar{\phi} \equiv \frac{\int_{\tau_0}^{\tau_0 + (2\pi/\omega)} \phi(\tau)\,\mathrm{d}\tau}{(2\pi/\omega)}, \tag{9}$$

$$\langle\phi\rangle \equiv \int_0^1 \phi\,\mathrm{d}Y.$$

In the above, ϕ stands for a physical variable; and subscript ss denotes the case of time-independent boundary condition, i.e. $\varepsilon = 0$. The amplitude and cycle-mean value of the oscillating ϕ are represented, respectively, by $A(\phi)$ and $\bar{\phi}$, and the vertically averaged value of ϕ is shown by $\langle\phi\rangle$.

The instantaneous, y-plane averaged heat transfer rate for the present conjugate system at an arbitrary vertical plane $X=a$ can be expressed by the Nusselt number in the fluid region, i.e.

$$Nu]_{X=a} = \frac{1}{A_r}\left(\frac{S_C+1}{S_C}\right)\int_0^1\left[\frac{\partial\theta}{\partial X} - (Ra\,Pr)^{1/2}U\theta\right]_{X=a}\mathrm{d}Y, \tag{10a}$$

where $S_C \equiv k_r/A_W$, which denotes the non-dimensional thermal conductance.

At the interior surface of the wall ($X = 1/A_r$), Nu can also be computed by the temperature gradient in the solid portion,

$$Nu_{X=1/A_r} = \frac{k_r}{A_r}\left(\frac{S_C+1}{S_C}\right)\int_0^1\left(\frac{\partial\theta}{\partial X}\right)_{X=(1/A_r)^+}\mathrm{d}Y. \tag{10b}$$

Obviously, the difference between the height-averaged temperature T_{int} at the interior surface ($X = 1/A_r$), and T_{ext} ($\equiv T_e + \Delta T_e \sin ft$) at the exterior surface ($X=(1+A_W)/A_r$) of the wall reflects the finite-wall effect. It is known that, inside the solid, the temperature field is principally a function of x, and the y-dependency of temperature is mild (see [11,17]). The ratio of the cycle-averaged values of T_{int} and T_{ext}, above the constant cold-wall temperature, is denoted by β, i.e.

$$\beta \equiv \frac{T_i - T_C}{T_e - T_C}$$

The conventional definition of the Nusselt number Nu_f for the fluid-only cavity can be re-written as

$$Nu_f \equiv \frac{1}{A_r}\int_0^1\left(\frac{\partial(\theta/\beta)}{\partial X} - (Ra\,Pr)^{1/2}U\frac{\theta}{\beta}\right)_{X=a}\mathrm{d}Y = \frac{1}{\beta}\left(\frac{S_C}{S_C+1}\right)Nu_{X=a}. \tag{11}$$

In the limit of an infinitely thin, perfectly conducting wall, i.e. for the benchmark model [1], $S_C \to \infty$ and $\beta \to 1.0$, thereby $Nu_f\rfloor_{X=1/A_r} \to Nu]_{X=1/A_r}$.

3. Results

3.1. Steady-state ($\varepsilon=0$) temperature at the interior surface of the wall

Here, the finite-wall effect for the non-pulsating boundary condition ($\varepsilon=0$) is delineated. The key quantity is the temperature at the interior surface of the wall, $\langle T_i\rangle[\equiv \int_0^1 \theta(X=1/A_r, Y)\mathrm{d}Y]$. In the steady state, the energy balance calls for

$$\left[\int_0^H k_f\left(\frac{\partial T}{\partial x}\right)_{x=L}\mathrm{d}y\right]_{\text{fluid}} = \left[\int_{\longleftrightarrow 0}^{\longleftrightarrow H} k_s\left(\frac{\partial T}{\partial x}\right)_{x=L}\mathrm{d}y\right]_{\text{solid}}, \tag{12}$$

which leads to the following relationship, with the afore-described temperature profile $T(x)$ in the solid,

$$\int_0^1\left(\frac{\partial\theta}{\partial X}\right)_{X=(1/A_r)^-}\mathrm{d}Y = S_C(1-\beta). \tag{13}$$

Therefore, the conventional Nusselt number Nu_f, defined for the fluid-side at the interior surface, is

$$Nu_f \equiv \frac{1}{A_r\beta}\int_0^1\left(\frac{\partial\theta}{\partial X}\right)_{X=(1/A_r)^-}\mathrm{d}Y = \frac{S_C(1-\beta)}{A_r\beta} \tag{14}$$

For steady-state buoyant convection, with the finite-wall effect incorporated, several preceding reports provided empirical relations stipulating Nu_f. For example, Kaminski and Prakash [11], by employing a lumped parameter approach, arrived at an expression for Nu_f as a function of Ra_i, i.e. the internal Ra based on the temperature difference over the fluid portion, $Ra_i = \alpha g(T_i - T_C)H^3/\nu\kappa$. A more comprehensive formula was derived here by generalizing the correlation of Berkovsky–Polevikov [17] to account for the variations in Pr and A_r, i.e.

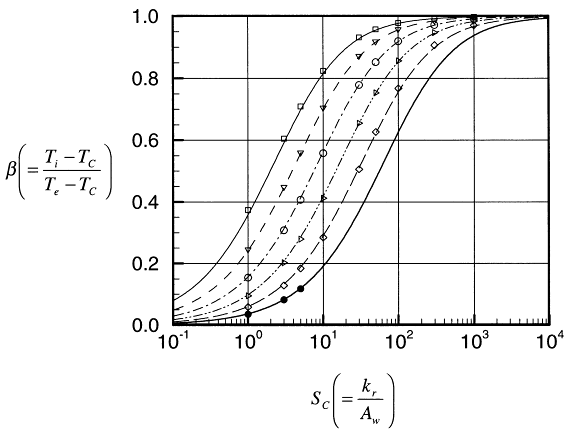

Fig. 2. Estimation of the temperature T_i at the interior surface of the wall. Lines denote results from Eq. (16), and symbols show the full numerical computations. —, $Ra = 10^4$; - - - -, $Ra = 10^5$; – -– - –, $Ra = 10^6$; – - - –, $Ra = 10^7$; – – –, $Ra = 10^8$; —, $Ra = 10^9$; □, $Ra = 10^4$; ▽, $Ra = 10^5$; ○, $Ra = 10^6$; ▷, $Ra = 10^7$; ◇, $Ra = 10^8$; •, $Ra = 10^9$.

$$Nu_{\mathrm{f}} = 0.18\left(\frac{Pr}{0.2+Pr}\,Ra_{\mathrm{i}}\right)^{0.29} A_r^{0.13}, \tag{15}$$

for which, $1.0 < A_r < 2.0$, $10^{-3} < Pr < 10^5$, $(Pr/0.2+Pr)Ra_{\mathrm{i}}\,A_{\mathrm{r}}^{-3} > 10^3$.

Combining Eqs. (14) and (15) yields

$$0.18\left(\frac{Pr}{0.2+Pr}\,\beta Ra\right)^{0.29} A_r^{0.13} = \frac{S_{\mathrm{C}}(1-\beta)}{A_r\beta}. \tag{16}$$

Eq. (16) poses a non-linear algebraic equation for the unknown β. By resorting to the interpolation method, numerical solutions can be acquired for β for a given set of (Ra, S_{C}) in Eq. (16). Exemplary results for the solutions to Eq. (16) are exhibited in Fig. 2 in lines, and, for comparison purposes, the results based on the full numerical solutions to the Navier–Stokes equations (Eqs. (1)–(5), (6a), (6b), (6c) and (6d)), are also illustrated by symbols. It is evident that the results from Eq. (16) and the Navier–Stokes solutions are in close agreement. The foregoing exercises give credence to the validity of the above simple analysis, which basically assumes a one-dimensional-type heat conduction in the horizontal direction within the finite-thickness solid wall. It also underscores the fact that, for the given externally specified parameter set, the height-averaged temperature T_{i} at the interior surface as well as the effective heat transport rate can be estimated by solving the algebraic Eq. (16). It is instructive to have physical interpretations of the qualitative behavior of β. As mentioned earlier, when the wall thickness is vanishingly thin ($A_{\mathrm{W}} \to 0$) or the thermal conductivity of the solid is very large ($k_r \to \infty$), the parameter $S_{\mathrm{C}} \to \infty$, which leads to $\beta \to 1$, i.e. $T_{\mathrm{i}} \to T_{\mathrm{e}}$ as shown in Fig. 2. Obviously, this corresponds to the standard benchmark model [1]. In the opposite limit of a very thick wall ($A_{\mathrm{W}} \gg 1$) or a poor thermal conductor (k_r: small), S_{C} becomes small, which indicates that the temperature contrast $(T_{\mathrm{i}} - T_{\mathrm{C}})$ over the fluid portion is substantially reduced. In this limiting case, the bulk of the externally imposed temperature difference $(T_{\mathrm{e}} - T_{\mathrm{C}})$ is consumed to offset the temperature drop over the solid wall $(T_{\mathrm{e}} - T_{\mathrm{i}})$. For a given value of S_{C}, the influence of Ra is of interest. When Ra is large, convection is the primary element in the fluid. In order to conserve the same amount of heat transport in both

Table 1
Major parameters for the four cases computed

Case	k_r	τ_{d}	$(\varepsilon_{\mathrm{d}}/\varepsilon_{\mathrm{i}})\mathrm{i},\omega_r$	β	ω_r	C_{i}
1	100	0.2646	0.962	0.982	0.77	1.113
2	10	2.646	0.633	0.854	0.68	0.876
3	1	26.46	0.085	0.418	0.46	0.431
4	0.1	264.6	10^{-4}	0.098	–	0.101

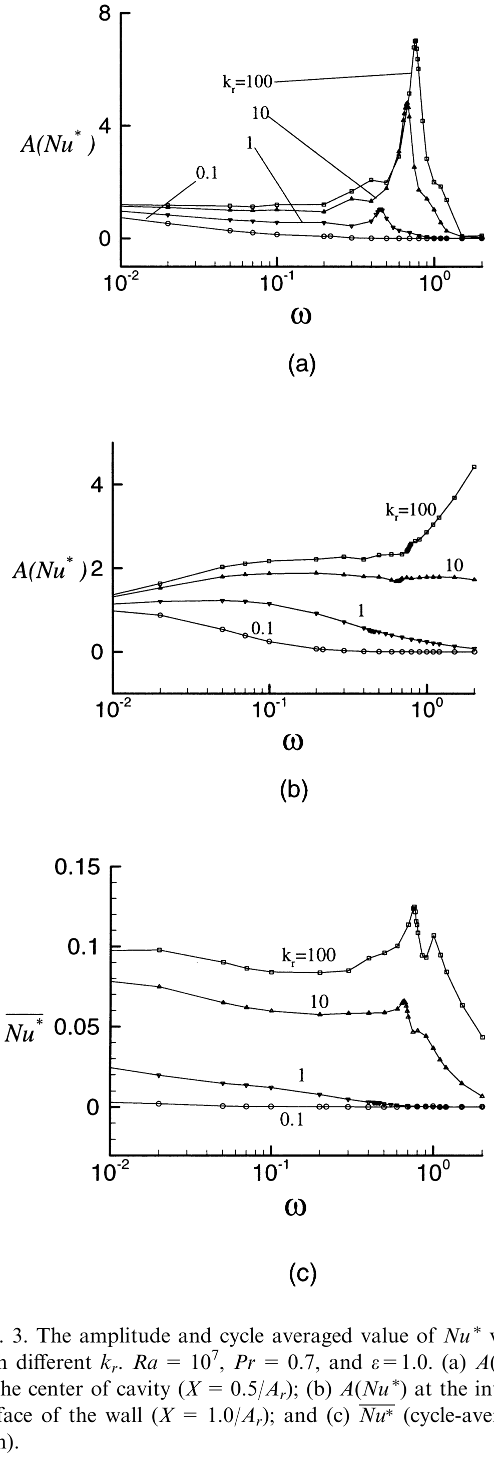

Fig. 3. The amplitude and cycle averaged value of Nu^* vs. ω, with different k_r. $Ra = 10^7$, $Pr = 0.7$, and $\varepsilon = 1.0$. (a) $A(Nu^*)$ at the center of cavity ($X = 0.5/A_r$); (b) $A(Nu^*)$ at the interior surface of the wall ($X = 1.0/A_r$); and (c) $\overline{Nu^*}$ (cycle-averaged gain).

the fluid and solid regions, the relative magnitude of $(T_i - T_C)$ decreases in comparison to $(T_e - T_i)$. These rationalizations are consistent with the temperature data displayed in Fig. 2.

3.2. The finite-wall effect on time-dependent interior convection ($\varepsilon \neq 0$)

The prominent flow characteristics in the quasi-steady periodic state are now examined. Specifically, four values of k_r, in the range $0.1 \leq k_r \leq 100$, are selected for full Navier–Stokes numerical computations (see Table 1).

The effect of the finite-thickness wall may be gauged by the conductive timescale t_d for a solid of thickness D and of thermal conductivity k_s, $t_d = D^2(\rho C)_s/k_s$. In accordance with the present scheme of non-dimensionalization, the dimensionless conductive time scale τ_d can be expressed as

$$\tau_d = \frac{(\rho C)_r}{k_r}(Ra\,Pr)^{1/2}\left(\frac{A_W}{A_r}\right)^2. \tag{17}$$

The values of τ_d are listed in Table 1 for the cases computed.

The series of comprehensive numerical results are processed to illustrate the behavior of $A(Nu^*)$, i.e. the amplitude of the oscillating, y-averaged Nusselt number Nu^*, versus the imposed pulsation frequency ω. Following the procedure of Lage and Bejan [3], the plots in Fig. 3a are for the central plane ($X = 0.5/A_r$). It is discernible that $A(Nu^*)$ at the central plane shows a peak at a particular value of ω. The existence of such a peak in $A(Nu^*)$ was interpreted to be resonance [3,7]. The present results under the finite-wall effect are consistent with the above-stated well-established concept of resonance, which had been discussed in the case of a completely conducting, infinitely thin wall (this case will hereafter be referred to as the canonical model of Kazmierczak and Chinoda [2]). For $k_r = 100$, resonance is seen at $\omega_r \cong 0.77$, which is almost identical to the value of the resonance frequency for the canonical model [8]. This is not unexpected since, as emphasized earlier, when k_r is very large, the dynamical role of the wall becomes similar to that of the canonical model. The numerical data of Fig. 3a show that, as k_r decreases, the peak value of $A(Nu^*)$ decreases and the resonance frequency also decreases slightly. These explicit manifestations of the finite-wall effect will be probed in the following sections.

It is also interesting to inspect the $A(Nu^*)$–ω plots at the interior surface of the wall ($X = 1/A_r$), as exhibited in Fig. 3b. Here, it must be noted that the information at the interior surface is important for the fluid convection because the fluid feels directly the pulsating boundary condition at the interior surface. When k_r is very large ($k_r = 100$), $A(Nu^*)$ gradually increases with ω for $\omega < \omega_r$ and increases steeply for $\omega > \omega_r$. This is consistent with the canonical model. But, as k_r becomes smaller, different results are shown. When $k_r = 10$, $A(Nu^*)$ remains fairly uniform with ω. Moreover, for smaller values of k_r, $A(Nu^*)$ slightly decreases with ω. The conductive-penetration timescale τ_d for large k_r is smaller than the period of pulsation $(2\pi/\omega)$; thus, the thermal impact that is delivered at the interior surface of the wall is less affected by the finite wall. On the contrary, when k_r is small, τ_d is larger than the period of pulsation; thus, the entire thermal impact can not be felt throughout the wall during a period of pulsation. In particular, for large ω, the period of pulsation becomes much smaller, and the finite-thickness wall acts like a regulator or a damper to attenuate the externally applied rapidly varying thermal loading. The alterations in boundary temperatures tend to be restricted to a small distance into the wall from the exterior surface. For the fluid in the neighborhood of the interior surface, the changes in the external temperatures are not felt, and $A(Nu^*)$ becomes vanishingly small. The gain in heat transport, time-averaged over a cycle, relative to the non-oscillating case is exhibited in Fig. 3c. When k_r is large, appreciable gains in $\overline{Nu^*}$ are seen. However, as k_r decreases, the gain in time-averaged heat transport is meager, as can easily be anticipated.

3.3. Temperature oscillation at the interior surface of the wall ($\varepsilon \neq 0$)

When the temperature at the exterior surface of the wall θ_{ext} contains a pulsating component, i.e. $\varepsilon \neq 0$ in Eq. (6c), the corresponding non-dimensional height-averaged temperature at the interior surface of the wall θ_{int} (at $X = 1/A_r$) can be written as

$$\theta_{int} = \beta + \varepsilon_i \sin(\omega\tau + \gamma_i) \tag{18}$$

in which ε_i and γ_i denote, respectively, the amplitude and phase lag of the pulsating part of θ_{int}.

The strategy here is to consider, in the first stage, the case when the thickness of the wall is very large, $A_W \gg 1$. Then, θ_{int} can be determined by obtaining an analytical solution to the conduction equation. In the next stage, when the thickness of the wall is finite, θ_{int} will be determined by allowing modifications due to convective activities in the fluid-portion of the cavity.

3.3.1. For a large-thickness wall ($A_W \gg 1$)

The non-dimensionalized, one-dimensional versions of Eqs. (5) and (6c) read

$$\frac{\partial\{(\rho C)_r\theta\}}{\partial\tau} = k_r\left(\frac{1}{Ra\,Pr}\right)^{1/2}\frac{\partial^2\theta}{\partial X^2}, \tag{19}$$

subject to

$$\theta\left[\frac{1}{A_r}(1+A_{\mathrm{W}}),\tau\right] = 1+\varepsilon\sin(\omega\tau), \quad \text{and} \qquad \theta[X,\tau] = \text{finite} \tag{20}$$

This problem setup is analogous to the well-documented Stokes' second problem (e.g. Schlichting [18]), which describes the response of an infinite viscous fluid to a rectilinearly oscillating infinite flat plate.

The solution to Eqs. (19) and (20) is found

$$\theta(\xi,\tau) = 1+\varepsilon\exp\left\{-\sqrt{\frac{(\rho C)_r\omega}{2k_r}}(Ra\,Pr)^{1/4}\xi\right\} \sin\left\{\omega\tau-\sqrt{\frac{(\rho C)_r\omega}{2k_r}}(Ra\,Pr)^{1/4}\xi\right\}, \tag{21}$$

in which $\xi \equiv (1+A_{\mathrm{W}})/A_r - X$. Consequently, the amplitude of temperature oscillation ε_{d} at an arbitrary location $\xi=\xi_{\mathrm{d}}$ inside the wall is shown to be

$$\frac{\varepsilon_{\mathrm{d}}}{\varepsilon} = \exp\left\{-\sqrt{\frac{(\rho C)_r\omega}{2k_r}}(Ra\,Pr)^{1/4}\xi_{\mathrm{d}}\right\} = \exp\left\{-\sqrt{\frac{\omega\tau_{\mathrm{d}}}{2}}\right\}, \tag{22}$$

in which τ_{d} indicates the (dimensionless) conduction timescale as shown in Eq. (17).

It follows that the distance $\xi=\delta$ from the exterior surface to the location where $\varepsilon_{\mathrm{d}}/\varepsilon$ falls to $1/e^2$ can be estimated to be

$$\delta = 2\sqrt{\frac{2k_r}{(\rho C)_r\omega}}(Ra\,Pr)^{-1/4}. \tag{23}$$

The applicability of the above-stated large-thickness model is subject to verification. Exemplary results for $\varepsilon_{\mathrm{d}}/\varepsilon$ calculated based on Eq. (22) are compared in Fig. 4 against the numerical data obtained by solving the full Navier–Stokes equations. As is clear, when $k_r=1$ (see Fig. 4a), the results of the large-thickness conduction model are in close agreement with the complete numerical solutions. This implies that, in this case, the determination of the solid interior temperatures is dominated by conduction. It is evident that ε_{d} decays fast as the distance from the exterior surface increases. As k_r increases (see Fig. 4b for $k_r=10$), $\varepsilon_{\mathrm{d}}/\varepsilon$ determined from the Navier–Stokes equations takes larger values than that from Eq. (22), reflecting the fact that the exterior-surface temperature penetrates with more ease into the solid. Since both θ_{int} and ε_{d} are not small, buoyant convective activities in the fluid are invigorated. Therefore, the discrepancy between the conduction-based large-thickness model of Eq. (22) and the full y-dependent Navier–Stokes numerical solution is appreciable. Also, because convection plays a bigger role, ε_{d} takes larger values at higher vertical locations (large y-values) in Fig. 4b. The inadequacy of the large-thickness conduction model is apparent when k_r is very large (see Fig. 4c for $k_r=100$). In this case, the solid wall approaches a perfect conductor; therefore, the difference between θ_{ext} and θ_{int} narrows, i.e. $\varepsilon_{\mathrm{d}}/\varepsilon \to 1$, and the y-dependence is relatively weak. Alternatively stated, due to the largeness of k_{s}, the penetration time for the thermal effect to travel across the wall is much smaller than the period of pulsation of θ_{ext}. As expected, when k_r is very large, the imposed boundary condition tends to the idealized perfectly

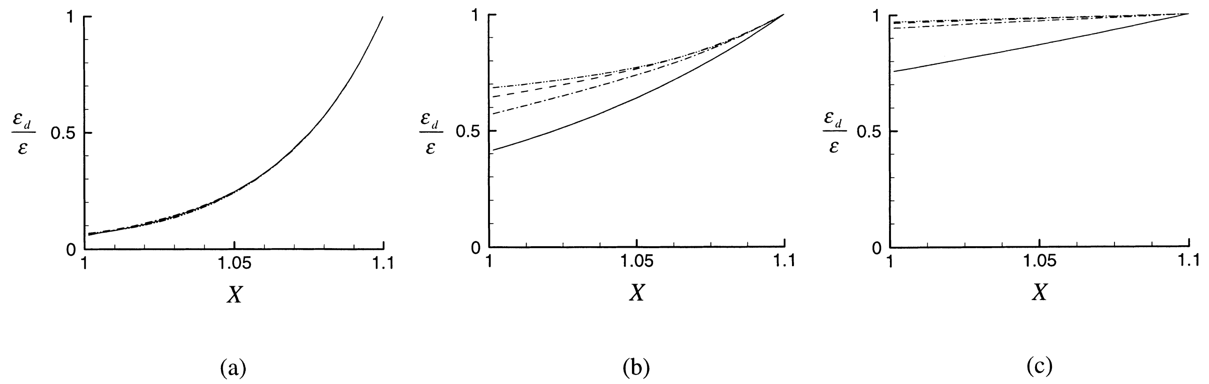

Fig. 4. Profiles of the amplitude of the oscillating temperature inside the solid wall. $Ra=10^7$, $\omega=0.6$. Solid lines denote the results of Eq. (22). The Navier–Stokes numerical results are: – -– - –, $Y=0$; – – – –, $Y=0.5$; and – - - –, $Y=1$. (a) $k_r=1$; (b) $k_r=10$; and (c) $k_r=100$.

conducting wall. Accordingly, for $k_r \gg 1$, the discrepancy between the large-thickness conduction model of Eq. (22) and the full numerical solution is reduced as k_r further increases. In summary, the applicability of the theoretical prediction of Eq. (22) increases for both k_r small or very large, and the performance of Eq. (22) is poor when $k_r \sim O(10)$ and when Ra is very large. A more quantitative criterion can be established by assessing the ratio of the conductive penetration time τ_d and the period of pulsation τ_p ($\equiv 2\pi/\omega$). This procedure incorporates all the effects of k_r, A_W and other parameters. Reviewing the numerical data, the validity of the large-thickness conduction model of Eq. (22) may be asserted when

$$\frac{\tau_d}{\tau_p} \le 10^{-3} \quad \text{or} \quad \frac{\tau_d}{\tau_p} \ge 1. \tag{24}$$

3.3.2. The convection-modified model

It is clear that the effect of convection should be included in any scheme to predict $\varepsilon_d/\varepsilon$ in the parameter space $10^{-3} \le \tau_d/\tau_p \le 1$, i.e. $k_r \sim O(10)$, from the above-stated analysis. Again, this points to the situation in which the influence of fluid convection, relative to the conduction in the solid, is significant in determining θ_{int}. To this end, an approximate fitting technique is devised by utilizing full-dress numerical results. The conduction-based prediction for $\varepsilon_d/\varepsilon$ of Eq. (22) is modified by adding a factor $f_m(\beta)$ to take into account the convective activities, i.e.:

$$\frac{\varepsilon_d}{\varepsilon} = \exp\left[-f_m\sqrt{\frac{\omega\tau_d}{2}}\right]. \tag{25}$$

By substituting the complete numerical solutions into $\varepsilon_d/\varepsilon$, f_m is evaluated, and the functional dependence of f_m on β is plotted in Fig. 5. The behavior of $f_m(\beta)$ is insensitive to Ra. An empirical formula can be produced by fitting a fourth-order polynomial to the

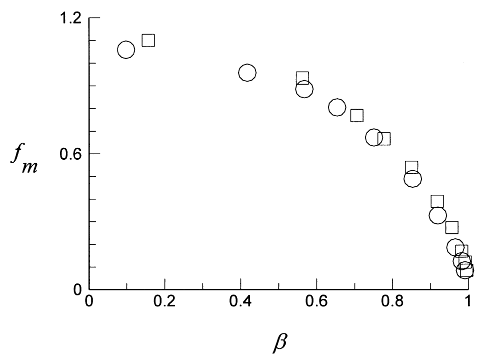

Fig. 5. The modifying factor f_m for the convection-modified model. ○, $Ra = 10^7$; and □, $Ra = 10^6$.

numerical data:

$$f_m = 1.0845 - 0.24978\beta - 0.18049\beta^2 + 0.71558\beta^3 - 1.309\beta^4. \tag{25b}$$

The reasonableness of the present approach is manifested in the exemplary plots of Fig. 6 for $Ra = 10^6$. As remarked previously, when k_r is small, the three sets of results are mutually consistent. When $k_r \ge O(10)$, the results of the large-thickness conduction model of Eq. (22) demonstrate appreciable deviations from the other two sets. To remedy this inadequacy, the results of the convection-modified model of Eq. (25) are in satisfactory agreement with the full numerical solutions.

3.4. Finite-wall effect on resonance frequency

In the preceding model developmental effort, Kwak and Hyun [7] asserted that resonance takes place when the externally applied forcing frequency matches the basic mode of natural frequency of the system. For the buoyant convection in an enclosure, the natural frequency is identified to be the fundamental mode of internal gravity oscillations, which are supported by the stable stratification of the enclosed fluid. It was demonstrated in the subsequent studies [7,9] that the theoretical predictions for the resonance frequency ω_r, based on the foregoing physical argument on internal gravity oscillations, were in broad agreement with the results of ω_r obtained by the full numerical solutions to the Navier–Stokes equations. These validations gave support to the physical rationalizations embedded in Kwak and Hyun [7].

Invoking the inviscid-fluid assumption for $Ra \gg 1$, the frequency of the basic mode of the internal gravity wave in a square can be computed, by using the present non-dimensional scheme ([19]), as

$$\omega_i = \sqrt{\frac{C_i}{2}}, \tag{26}$$

in which C_i indicates the average vertical gradient of density in the interior region of stratified fluid, namely, the strength of interior stratification. The numerically obtained values of C_i, in the range $0.2 \le Y \le 0.8$ at $X = 0.5/A_r$, are listed in Table 1. Here C_i is computed from the cycle-averaged solutions, rather than the basic state, because of the non-linearity at large value of ε [9]. The predicted values of ω_i of Eq. (26) were in good agreement with the numerically acquired values of ω_r.

Sequential pictures over a cycle are provided in Fig. 7 to demonstrate the evolutions of temperature and flow fields at resonance. As discussed by [8], the

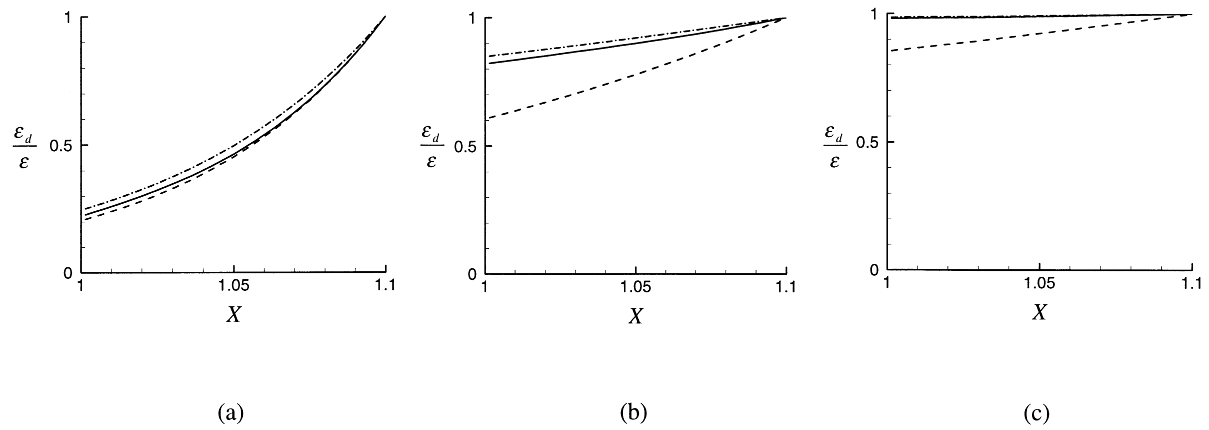

Fig. 6. Profiles of the amplitude of the oscillating temperature inside the solid wall. $Ra = 10^6$, $\omega = 10^6$. —, full Navier–Stokes solutions ($Y = 0.5$); – – – –, large-thickness conduction model; and –·–, convection-modified model. (a) $k_r = 1$; (b) $k_r = 10$; and (c) $k_r = 100$.

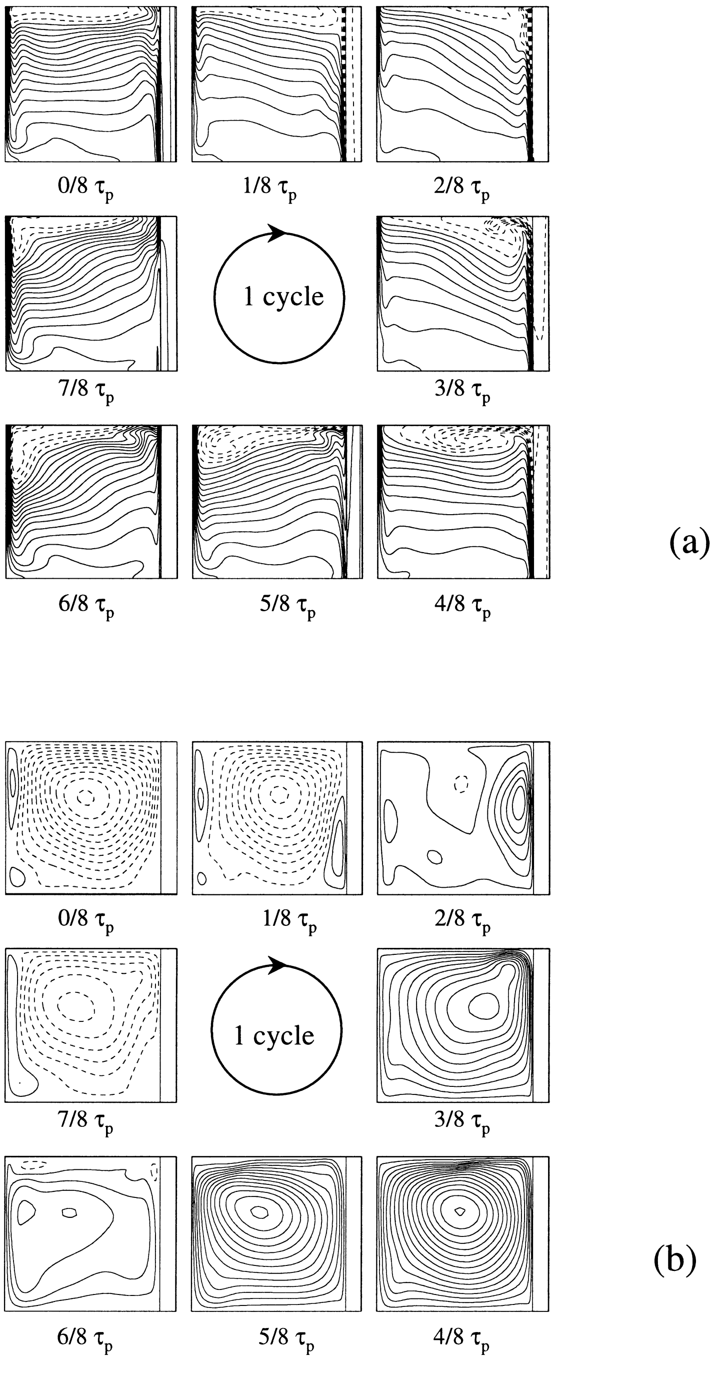

Fig. 7. Sequential pictures showing the evolutions of (a) temperature and (b) flow fields. $k_r = 100$; $\varepsilon = 1$; $\omega = 0.77$; and $Ra = 10^7$. Time instants are shown for each frame. In (a), dashed lines indicate $\theta \geq 1$. In (b), dashed lines indicate negative contour values.

tilting of the isotherms in the interior is in evidence, together with the cyclic motions.

4. Conclusions

A general formulation for enclosed buoyant convection with a vertical wall of finite-thickness has been presented. For the case of non-pulsating boundary temperature condition ($\varepsilon = 0$), a combination of analytical treatment and empirical relationship produces a simple formula to predict the temperature T_i at the interior surface of the wall. The predictions are shown to be consistent with the results based on full Navier–Stokes numerical solutions. Numerical computational results have been examined to describe the finite-wall effect when the temperature at the exterior surface of the hot vertical wall has a pulsating component ($\varepsilon \neq 0$). The results establish that $A(Nu^*)$ at the central plane has a sharp peak at the resonance frequency ω_r. As k_r decreases, the resonance frequency decreases slightly and a substantial reduction is seen in the value of $A(Nu^*)$. These findings are qualitatively consistent with the earlier assertions on physical rationalizations of resonance phenomenon. The temperature oscillation at the interior surface of the wall is estimated reasonably well by a one-dimensional conduction model in the solid, together with the convection model in the fluid. An empirical correlation is proposed to depict the explicit finite-wall effect on the interior-surface temperature oscillations.

Acknowledgements

The authors are grateful to the referees for constructive and helpful comments. This work was supported by the NRL Project MOST, RRC (KOSEF) and Korea Energy Management Corporation, South Korea.

References

[1] G. de Vahl Davis, Natural convection of air in a square cavity: a benchmark numerical solution, Int. J. Numer. Methods Fluids 3 (1983) 249–264.
[2] M. Kazmierczak, Z. Chinoda, Buoyancy driven flow in an enclosure with time-periodic conditions, Int. J. Heat Mass Transfer 35 (1992) 1507–1518.
[3] J.L. Lage, A. Bejan, The resonance of natural convection in an enclosure heated periodically from the side, Int. J. Heat Mass Transfer 36 (1993) 2027–2038.
[4] J.M. Hyun, Unsteady buoyant convection in an enclosure, Adv. Heat Transfer 24 (1994) 227–320.
[5] B.V. Antohe, J.L. Lage, Amplitude effect on convection induced time-periodic horizontal heating, Int. J. Heat Mass Transfer 39 (1996) 1121–1133.
[6] B.V. Antohe, J.L. Lage, Experimental investigation on pulsating horizontal heating of an enclosure filled with water, ASME J. Heat Transfer 118 (1996) 889–896.
[7] H.S. Kwak, J.M. Hyun, Natural convection in an enclosure having a vertical sidewall with time-varying temperature, J. Fluid Mech. 329 (1996) 65–88.
[8] H.S. Kwak, K. Kuwahara, J.M. Hyun, Resonance enhancement of natural convection heat transfer in a square enclosure, Int. J. Heat Mass Transfer 41 (1998) 2837–2846.
[9] H.S. Kwak, K. Kuwahara, J.M. Hyun, Prediction of the resonance frequency of natural convection in an enclosure with time-periodic heating imposed on one sidewall, Int. J. Heat Mass Transfer 41 (1998) 3157–3160.
[10] D.M. Kim, R. Viskanta, Study of the effects of wall conductance on natural convection in differentially oriented square cavities, J. Fluid Mech. 144 (1984) 153–176.
[11] D.A. Kaminski, C. Prakash, Conjugate natural convection in a square enclosure: effect of conduction in one of the vertical walls, Int. J. Heat Mass Transfer 29 (1986) 1979–1988.
[12] W.J. Chang, H.C. Lin, Wall heat conduction effect on natural convection in an enclosure filled with a non-Darcian porous medium, Numer. Heat Transfer A 25 (1994) 671–684.
[13] K.H. Chung, J.M. Hyun, Transient natural convection in a cavity with walls of finite thickness, Numer. Heat Transfer A 32 (1997) 749–767.
[14] S.V. Patankar, Numer. Heat Transfer Fluid Flow, McGraw-Hill, New York, 1980.
[15] T. Hayase, J.A.C. Humphrey, R. Greif, A consistently formulated QUICK scheme for fast and stable convergence using finite-volume iterative calculation procedures, J. Comput. Phys. 98 (1992) 108–118.
[16] H.L. Stone, Iterative solution of implicit approximations of multidimensional partial difference equations, SIAM J. Numer. Anal. 5 (1968) 530–558.
[17] I. Catton, Natural convection in enclosures, Sixth International Heat Transfer Conference, Toronto, 6, 1979, pp. 13–43.
[18] H. Schlichting, Boundary Layer Theory, McGraw-Hill, New York, 1968.
[19] S. Paolucci, D. Chenoweth, Transition to chaos in a differentially heated vertical cavity, J. Fluid Mech. 201 (1989) 379–410.